

A novel 3D deformation measurement method under optical microscope for micro-scale bulge-test



Dan Wu^{a,*}, Huimin Xie^b

^a School of Mechanical Engineering and Mechanics, Ningbo University, Ningbo 315211, China

^b Key Laboratory of Applied Mechanics (AML), Department of Engineering Mechanics, Tsinghua University, Beijing 100084, China

ARTICLE INFO

Keywords:

Micro-scale
3D deformation measurement
Bulge-test
Gratings
Optical microscope

ABSTRACT

A micro-scale 3D deformation measurement method combined with optical microscope is proposed in this paper. The method is based on gratings and phase shifting algorithm. By recording the grating images before and after deformation from two symmetrical angles and calculating the phases of the grating patterns, the 3D deformation field of the specimen can be extracted from the phases of the grating patterns. The proposed method was applied to the micro-scale bulge test. A micro-scale thermal/mechanical coupling bulge-test apparatus matched with the super-depth microscope was exploited. With the gratings fabricated onto the film, the deformed morphology of the bulged film was measured reliably. The experimental results show that the proposed method and the exploited bulge-test apparatus can be used to characterize the thermal/mechanical properties of the films at micro-scale successfully.

© 2017 Elsevier Ltd. All rights reserved.

1. Introduction

With increasing applications of thin films in many areas [1–4], the mechanical property characterization of thin films is crucial. Conventional applied methods, such as the wafer curvature method based on the Stoney's formula and the nano-indentation method [5,6], have been applied to characterize the mechanical properties of the thin films. Although the wafer curvature method is easy to implement and applied to measure the residual stress of the films, it's hard to extract other properties of the films. The nano-indentation test can be used to characterize the elastic-plastic properties of the film, but influences of substrates can't be eliminated. So the above mentioned methods have limitations for the mechanical properties characterization of thin films.

To characterize the mechanical properties of free-standing films, micro-tensile test and bulge-test were developed. The micro-tensile test can measure the intrinsic properties of the films directly and constitutive behaviors with the increasing load applied [7]. Sharpe et al. proposed a micro-tensile test technique, which can measure the strain of free-standing films in micro-region based on the optical interferometric strain gauge method [8]. The strain can be exactly obtained with the interferometric method. Li et al. proposed a compact in situ micro tensile apparatus together with the scanning electron microscope (SEM) to characterize the mechanical properties of the free-standing films [9]. In this method gratings were fabricated on the films by focused ion beam milling, and the strain field can be extracted by the fabricated gratings.

The advantage of the SEM scanning moiré method is full field deformation measurement compared with optical interferometric strain gauge method.

Even though the micro-tensile test methods can satisfy the demand for the mechanical characterization of the free-standing films, some special requirements cannot be perfectly fulfilled, such as the measurement of polymer films. When buckling is more likely to occur [10], the out-of-plane displacement will bring difficulty to the measurement. Comparatively, bulge-test methods are more competent [11–13]. The mechanical properties of the film are determined from the related pressure-deflection theory [14–16].

The critical technique of the bulge-test method is the characterization of the out-of-plane deflection of the films [17]. Especially, for micro-scale bulge-test, the 3D deformation characterization is challenging [18,19]. Many research works have been carried out to provide techniques to characterize the 3D deformation in micro/nano scale [20]. The microscopic 3-D displacement field measurement by digital image correlation method has been proposed and the speckle patterns were obtained by two CCD cameras of the stereomicroscope [21]. Shi et al. [22] have proposed the fringe projection combined with the digital image correlation method to characterize the out-of-plane deformation of small objects. Wu et al. [23] characterized the 3D deformation of thin films in SEM by grating based method.

Even though the digital image correlation method is widely used in the measurement field, the image distortion induced from the mi-

* Corresponding author.

E-mail addresses: wudan@nbu.edu.cn (D. Wu), xiehm@mail.tsinghua.edu.cn (H. Xie).

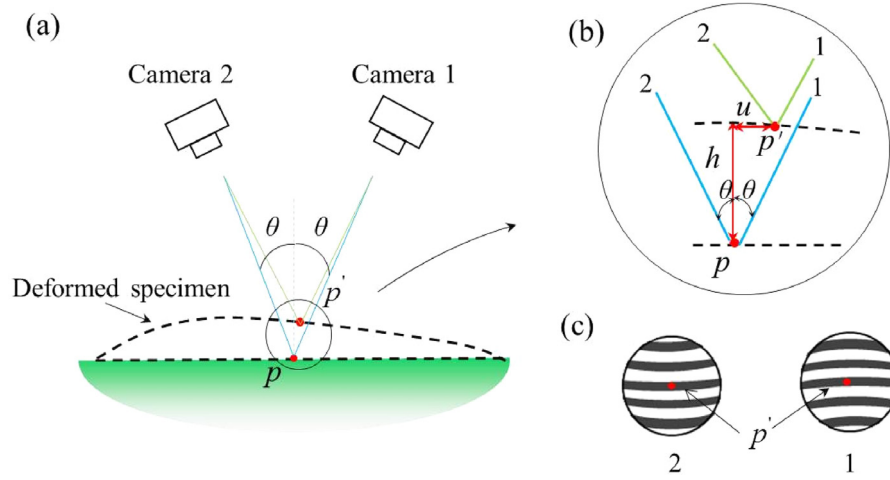


Fig. 1. A schematic of the basic principle of the proposed 3D deformation measurement method: (a) two symmetric CCDs are used to capture the grating images before and after deformation; (b) the point p moves to p' and the number 1 and 2 corresponds to the light path of camera 1 and 2; (c) the deformed grating images obtained by two CCDs.

croscopy imaging system will bring significant error to this method. This error is especially prominent for optical microscope due to small depth of field. So evaluation and elimination of errors are required, which is relatively complicated.

In this paper, we demonstrate a 3D deformation measurement method to characterize the deflection of the micro-scale bulge-test, which is integrated with the super-depth microscope. The 3D displacement fields of the deflected film were obtained, more than the morphology obtained by the white light interferometer [13]. This method is based on the grating based measurement method and the digital phase shifting technique. Compared with the SEM digital image correlation method [18], the grating based measurement method [24,25] is less affected by image distortion and drifting. With the proposed method, thermal/mechanical coupling bulge-test to the polyimide films was performed. The results indicate the feasibility of this method.

2. Theoretical background

2.1. Basic principles

The proposed method is based on gratings, so micro/nano-gratings need to be fabricated on the specimen before deformation. It is assumed that the specimen grating is uniform and the pitch is d , and the fringe is parallel to the y axis. The gratings along the x axis can be expressed by Fourier series as [26]:

$$I = A_0 + \sum_{n=1}^{\infty} B_n \cos \frac{2\pi n}{d} x + \sum_{n=1}^{\infty} C_n \sin \frac{2\pi n}{d} x \quad (1)$$

where I is the intensity of the specimen gratings, A_0 , B_n , C_n are constants, which can be determined from the fringe profile of the gratings. It is assumed that the specimen surface is flat before deformation. In our testing system, there are two digital cameras symmetric about the normal direction of the specimen surface (Fig. 1(a)). It should be noted that in this method the specimen is in micro-scale and far less than the distance from the CCD to the specimen surface. So it is approximately regarded that the two CCDs are symmetric about the normal of every point on the specimen surface. The approximation will bring slight deviation to the measurement, which will be discussed later in the text.

Due to the CCD is oblique to the specimen grating, the pitch of the grating image obtained by the two CCDs is $d' = d \cos \theta$. When the specimen deformed and the point p moves to p' (Fig. 1(b)), the displacement of the corresponding point p' in the grating image (Fig. 1(c)) obtained by camera 1 is $u - h \tan \theta$ (Fig. 1(b)). So the coordinate of $p' x_1 = x - h \tan \theta + u$. The displacement by camera 2 is $h \tan \theta + u$. The corresponding coordinate

of p' is $x_2 = x + h \tan \theta + u$. So the grating intensity obtained by the two cameras is expressed as:

$$\begin{cases} I_1 = A_0 + \sum_{n=1}^{\infty} B_n \cos \frac{2\pi n}{d'} x_1 + \sum_{n=1}^{\infty} C_n \sin \frac{2\pi n}{d'} x_1 \\ I_2 = A_0 + \sum_{n=1}^{\infty} B_n \cos \frac{2\pi n}{d'} x_2 + \sum_{n=1}^{\infty} C_n \sin \frac{2\pi n}{d'} x_2 \end{cases} \quad (2)$$

Here the two cameras are regarded as exactly the same, so the coefficients of the two formulas in Eq. (2) are the same. From Eq. (2), the in-plane displacement in x direction and out-of-plane displacement are included in the deformed grating images. u and h are related with the phases of the gratings. To extract the two components, the phases of the gratings are to be calculated. Digital moiré method was applied in the process to extract the phase information. Firstly, digital reference grating was generated by the computer program. The generated grating fringes are parallel to the y axis and the intensity of the sinusoidal grating can be expressed as:

$$I_0 = a_0 + b_0 \cos \frac{2\pi}{d_0} x + c_0 \sin \frac{2\pi}{d_0} x \quad (3)$$

where a_0 , b_0 , c_0 are constants, and d_0 is the pitch of the reference gratings. After superimposing the reference gratings with the specimen grating image obtained by camera 1, the results I' is obtained:

$$\begin{aligned} I' = I_0 I_1 = & a_0 A_0 + b_0 A_0 \cos \frac{2\pi}{d_0} x + c_0 A_0 \sin \frac{2\pi}{d_0} x + a_0 \sum_{n=1}^{\infty} B_n \cos \frac{2\pi n}{d'} x_1 \\ & + a_0 \sum_{n=1}^{\infty} C_n \sin \frac{2\pi n}{d'} x_1 + \frac{1}{2} (b_0 C_1 - c_0 B_1) \sin \left[\frac{2\pi}{d'} x_1 - \frac{2\pi}{d_0} x \right] \\ & + \frac{1}{2} (b_0 B_1 + c_0 C_1) \cos \left[\frac{2\pi}{d'} x_1 - \frac{2\pi}{d_0} x \right] \\ & + \frac{1}{2} \sum_{n=2}^{\infty} (b_0 C_n - c_0 B_n) \sin \left[\frac{2\pi n}{d'} x_1 - \frac{2\pi}{d_0} x \right] \\ & + \frac{1}{2} \sum_{n=2}^{\infty} (b_0 B_n + c_0 C_n) \cos \left[\frac{2\pi n}{d'} x_1 - \frac{2\pi}{d_0} x \right] \\ & + \frac{1}{2} \sum_{n=1}^{\infty} (b_0 C_n - c_0 B_n) \sin \left[\frac{2\pi n}{d'} x_1 + \frac{2\pi}{d_0} x \right] \\ & + \frac{1}{2} \sum_{n=1}^{\infty} (b_0 B_n + c_0 C_n) \cos \left[\frac{2\pi n}{d'} x_1 + \frac{2\pi}{d_0} x \right] \end{aligned} \quad (4)$$

It can be seen that the second line of Eq. (4) is the original reference and specimen grating structures. If d_0 approximately equals to d' ,

$1/d' - 1/d_0 \approx 0$. The frequency of the term expressed by the third line is much lower than the gratings. This term represents the moiré fringe system. The fourth and fifth lines are the multiplicity of the moiré fringes. The moiré fringe term can be thought as the fundamental frequency signal, and the rest terms the high frequency noise. For geometric moiré, whether the noise can be detected or not depends on the resolution of the detecting system. Due to the digital generated gratings were applied to form the moiré fringes, the noise can be distinguished from the moiré fringes. Thus filtering noise is a necessary step during fringe processing for this method. Assuming that high frequency terms in Eq. (4) are completely filtered out, the moiré fringes I_m can be expressed as:

$$\begin{cases} I_m^1 = A \cos \left[\frac{2\pi}{d'} x_1 - \frac{2\pi}{d_0} x + \varphi_0 \right] \\ I_m^2 = A \cos \left[\frac{2\pi}{d'} x_2 - \frac{2\pi}{d_0} x + \varphi_0 \right] \end{cases} \quad (5)$$

where A is the amplitude of the fringes and φ_0 is the initial phase. To obtain the displacement information included in Eq. (5), multi-step phase shifting method was used. Take four-step phase shifting as an example, and the phase φ of the fringe pattern can be obtained by:

$$\varphi = \arctan \frac{I_4 - I_2}{I_1 - I_3} \quad (6)$$

In Eq. (6), I_1, I_2, I_3 and I_4 are the shifted fringes with step of $0, \pi/2, \pi$ and $3\pi/2$, respectively. With the digital phase shifting method, the phases of the moiré fringes expressed by Eq. (5) are solved as:

$$\begin{cases} \varphi_1 = \frac{2\pi}{d'} (x - h \tan \theta + u) - \frac{2\pi}{d_0} x + \varphi_0 \\ \varphi_2 = \frac{2\pi}{d'} (x + h \tan \theta + u) - \frac{2\pi}{d_0} x + \varphi_0 \end{cases} \quad (7)$$

Consequently, the out-of-plane displacement h can be obtained by eliminating the unknown terms u in Eq. (7):

$$h = \frac{(\varphi_2 - \varphi_1)d}{4\pi \tan \theta \sec \theta} \quad (8)$$

Eq. (8) gives out the expression for the out-of-plane displacement. From Eq. (8), the out-of-plane displacement can be estimated from the phases of the gratings. So the key point is calculating of the grating phases.

2.2. Accuracy analysis

It has been assumed the two CCDs are symmetric about the normal direction of the specimen surface. Because the view field is in micro-scale and far less than the distance from the CCD to the specimen surface, θ is approximately equal at each point. The error from this approximation can be estimated as follows: assuming that the diameter of the specimen is $100 \mu\text{m}$, the distance from the specimen surface to the imaging target is estimated 200 mm , and θ is 45° . From the center to the edge of the specimen, $\Delta \tan \theta$ (the variation of the tangent value of θ) is estimated 1.4×10^{-3} . From Eq. (8), the error to h :

$$\Delta h_1 = \frac{(\varphi_2 - \varphi_1)d(1 + \sin^2 \theta)}{4\pi \tan \theta \sin \theta} \Delta \theta \quad (9)$$

Δh_1 represents the error induced by deviation of θ . The relative error $\Delta h_1/h \approx \Delta \theta / \tan \theta$ and approximates 1.4×10^{-3} . So the error induced by neglecting the deviation of θ is very small.

From Eq. (8), the error of h mainly comes from the uncertainty of the calculated phase φ . If the high frequency terms in Eq. (4) have not been filtered out completely during the fringe processing, it would bring disturbance to the calculating of the moiré fringe phases. Appropriate filtering windows need to be selected to filter out the noise. It has been claimed that the phase shifting method has the displacement sensitivity of $1/100$ of the grating pitch [27]. The error of h comes from the phase shifting algorithm can be expressed as:

$$\Delta h_2 = \frac{(\Delta \varphi_2 - \Delta \varphi_1)d}{4\pi \tan \theta \sec \theta} \quad (10)$$

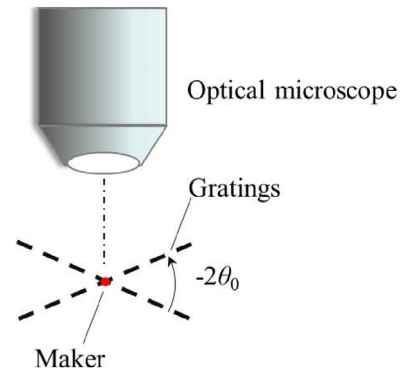


Fig. 2. A schematic of the 3D measurement principle integrated with the optical microscope.

The displacement of one grating pitch represents one order moiré fringe, so $\Delta \varphi_1 = \Delta \varphi_2 \approx 2\pi/100$. The relative error $\Delta h_2/h$ induced by the phase shifting algorithm can be estimated from Eq. (10). $\Delta h_2/h = (\Delta \varphi_2 - \Delta \varphi_1) / (\varphi_2 - \varphi_1)$. It is worth noting that due to the moiré fringe numbers increase with the grating frequency at the same deformation field, and the relative error is decreasing with the increase of the grating frequency.

3. Method description

3.1. The 3D measurement method for bulge-test

The proposed 3D measurement method applied for micro-scale bulge-test is based on optical microscope, it has been noted that the measurement is based on two cameras of symmetric angles on the specimen (Fig. 1). This can be achieved by tilting the specimen symmetrically, and transforming the relative angle between the optical path of the microscope and the specimen surface. During the movement of the specimen, a marker was captured and kept at the center of the view field (Fig. 2). The grating patterns were captured at two symmetric tilting angles θ_0 and $-\theta_0$.

To fulfill the tilting of the specimen, a self-developed apparatus providing arbitrary angle from 0 to 90° was applied (Fig. 3(a)). For every load step, two grating images observed at two symmetric tilting angles were captured (Fig. 3(b)).

3.2. Apparatus

A schematic of the designed micro-scale bulge-test system integrated with the microscope is shown in Fig. 4(a). The system is comprised of four parts, including the air bump, control box, bulge-test chamber and the super-depth microscope (KEYENCE VHX-500FE).

The air bump can be manipulated manually and the inflation speed is controlled by the valve of an air bag situated in the control box (Fig. 4(a)). The control box is in charge of the pressure and temperature of the chamber during the experiment. The pressure transducer is in the range of $0 \sim 500 \text{ kPa}$. The bulge-test chamber is cylindrical, and the inner diameter and the height are 71 mm , 60 mm respectively. There is a heating element (220 V , 100 W , $25 \times 30 \text{ mm}^2$) placed in the bottom of the chamber. The temperature of the chamber can reach 190°C , which can be measured by the thermocouple. A circular copper plate with a through hole was placed in the upside of the chamber and sealed with the chamber by the silicone rubber ring (Fig. 4(b)). The thermal conductivity of the copper plate is good and the heat can be transmitted to the film rapidly. The sealing is maintained by the mating threads of the cap on the chamber. Pre-tightening force was imposed to the cap on the chamber before experiment.

Before conducting the bulge-test experiment, the gratings were fabricated on the polymer film on metal substrate, which was processed with

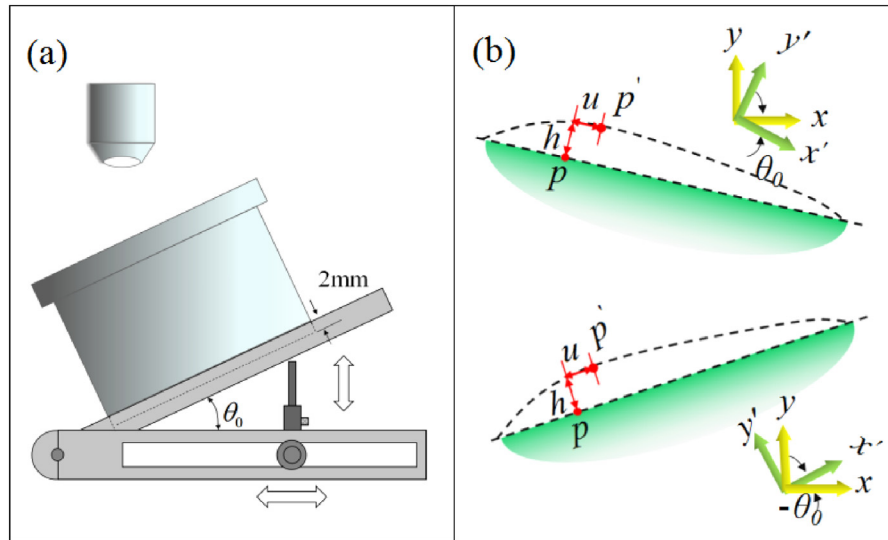


Fig. 3. (a) A schematic of the bulge-test chamber placed on the tilting apparatus; (b) The displacement of the particle on the film of different tilting angle.

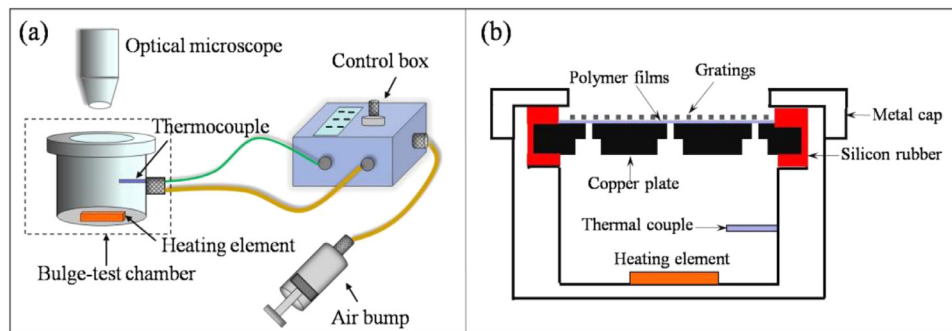


Fig. 4. (a) A schematic of the bulge-test system, (b) the cross section of the bulge-test chamber marked by the dashed box shown in (a).

through holes. Then the substrate with film was adhered to the copper plate by high temperature adhesive.

3.3. Sample preparation

The tested polyimide films are frequently used in many fields, e.g. as the substrate material of flexible circuits, and have excellent heat resistant performance superior to other polymer films. In service process of the polyimide films, heat is inevitably produced and may affect the mechanical properties of the polyimide films. So it's necessary to characterize the mechanical properties of films under thermal/mechanical coupling environment.

The moiré deflectometry has been applied for the measurement of polymer films [28]. The principle of this method is deflection of incoherent collimated light and the light path arrangement is relative simple compare with interferometry. However, this method is limited to micro-scale measurement.

The non-interferometric method applied to the micro-scale measurement here is based on the grating measurement method. The sample preparation process includes: Firstly, the silicone pressure sensitive adhesive is uniformly coated on the polyimide film. Because the thickness of the adhesive is within a few micrometers, and the adhesive is not completely solidified, the influence of the adhesive to the film is neglected. The polyimide film is carefully pasted onto the metal substrate. The substrate is drilled with a through-hole (diameter 450 μm) beforehand and then polished to specular gloss to avoid air leakage of the bulge-test. The bonding of the film and the metal substrate by the adhesive is strong enough in the measured pressure range (0~100 kPa). It would be

proven in the following content that the interface delamination has not taken place in the measured pressure range. At the same time, it should be noted that the adhesive can withstand the tested temperature in the experiment.

The critical step for the grating based measurement method is the grating fabrication. Grating fabrication techniques include holographic interferometry, nanoimprint, focused ion beam milling, et al. [24,25,29]. Each of these approaches has its advantages and disadvantages. Holographic interferometry is efficient but the light path is complex relatively. Nanoimprint brings residual photo-resist, which is not proper for application of films.

Here photolithography was applied to fabricate gratings on the polymer films. Firstly the photo-resist was spinning coated on the surface of the film, and the thickness of the photo-resist film is less than 1 μm . Afterwards, a photolithography process was conducted to duplicate the 80 lines/mm gratings on the copper template to the photo-resist film. Fig. 5(a) and (b) show the grating fabrication process. From Fig. 5(d) there was no photo-resist residual in the developed area. It is regarded that the influence of the photo-resist on the polyimide film can be neglected.

3.4. Bulge-test experiment

The bulge-test system is shown in Fig. 6. The pressure and temperature value of the chamber are displayed on the control box. The polyimide films were tested by the bulge-test system at room temperature (25 °C) and 150 °C respectively. The gratings (photo-resist) on the film could bear the test temperature. For high temperature measurement, the

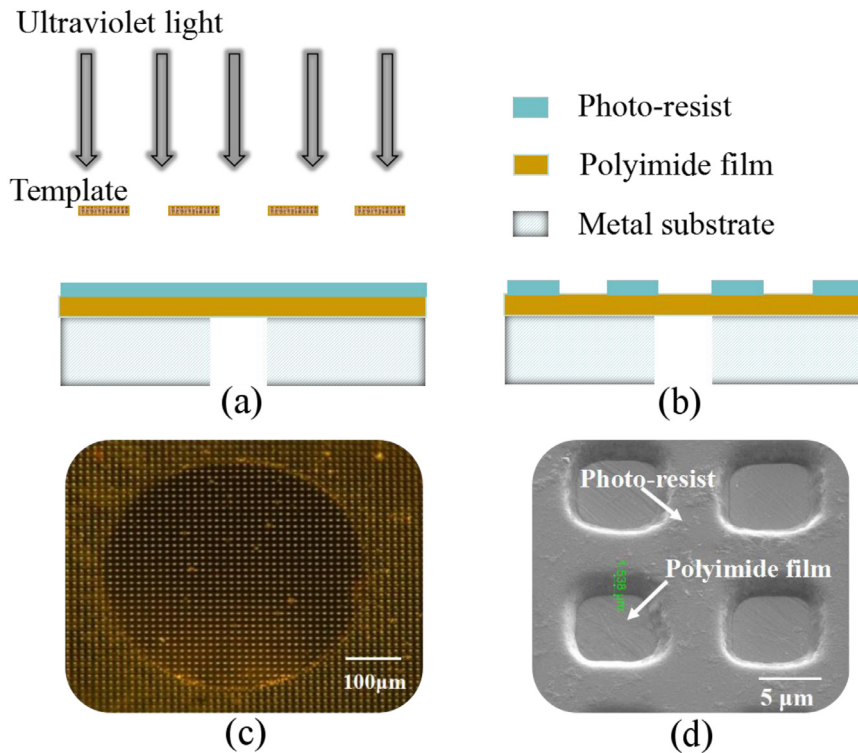


Fig. 5. The gratings fabrication process, (a) and (b) the photolithography process, (c) and (d) the gratings (80 lines/mm) observed by the optical microscope (tilting angle 30°) and SEM (tilting angle 30°) respectively.



Fig. 6. The bulge-test system, including a control box, an air bump, a microscope and a bulge-test chamber.

air was pumped after the temperature arrives to the set values. The temperature of the specimen is almost not influenced during the inflation. The inflation speed was controlled by the valve and the pressure was increased slowly. The proper magnification of the microscope for the measured specimen is set at $\times 200$. The pitch d' of the captured grating images are 12 pixels, thus the frequency of the grating is $1/12$. Due to the obliquity of the specimen, the specimen was out-of-focus and with the super-depth synthesis function of the microscope, clear images of the bulged membrane were obtained with the stepping motor of the microscope. In this experiment, the tilting angles were set at 30° and -30° .

4. Results and discussions

Two grating images captured during the experiment are shown in Fig. 7(a) and (b). The specimen is kept at 25°C and tested at pressure from 0 to 100 kPa. It can be seen that excellent contrast were formed. With the proposed three-dimensional deformation measurement method, the displacement information can be extracted from the grating images. The corresponding moiré fringe patterns formed by the superposition of the specimen gratings on the reference gratings (the pitch d_0 is 11 pixels) are shown in Fig. 7(c) and (d). The fringe patterns were processed with Gaussian blurring to filter high frequency terms. Eight step phase-shifting was applied to calculate the phase of the gratings and the step is $\pi/4$. The accuracy is improved by increasing the shifting steps. With the calculated phase of the grating at tilting angle 30° and -30° , the bulge deflection of the membrane can be obtained from Eq. (8).

The moiré fringes obtained from 0 to 100 kPa are shown in Fig. 8. It is obvious that the curvature of the fringes is increasing with the load. The displacement of the film is visualized by the moiré fringes. It has been claimed that the displacement accuracy of the phase shifting method is $1/100$ of the grating pitch [27]. The grating pitch is about $12 \mu\text{m}$, so the displacement accuracy estimated from Eq. (10) is $0.18 \mu\text{m}$.

The calculated bulge deflection of the membrane at 25°C and 100 kPa is shown in Fig. 9. It should be noted that in the measured pressure range, the interface between the film and the metal substrate has not delaminated. It has been repeatedly tested in the range of 100 kPa, and confirmed that delamination has not taken place. When the pressure was increased further, delamination would take place. From Fig. 9, bubbles occurred around the hole of the bulge-test when the pressure was increased to 140 kPa, indicating that the interface delamination between the film and the substrate.

From the measured bulge profile, the maximum deflection can be determined. For the bulge-test membrane, the bulge deflection is used for the evaluation of the mechanical properties of the film. The relationship

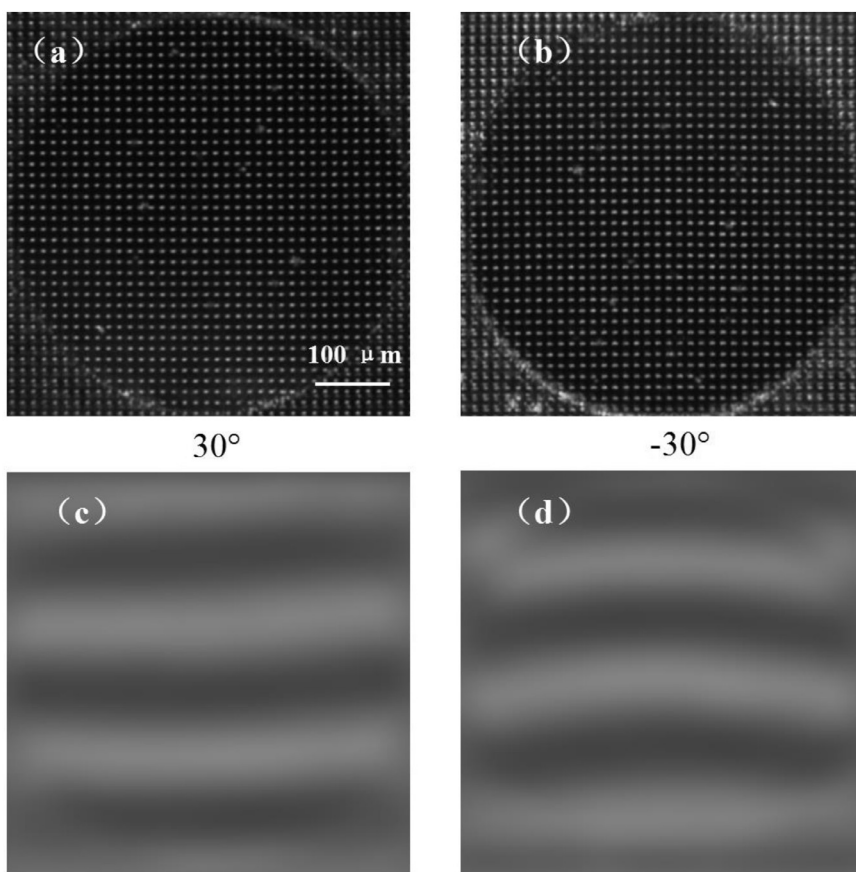


Fig. 7. (a) and (b) are the grating images obtained during the experiment at tilting angles 30° and -30° respectively; (c) and (d) are the corresponding digital moiré fringes of (a) and (b).

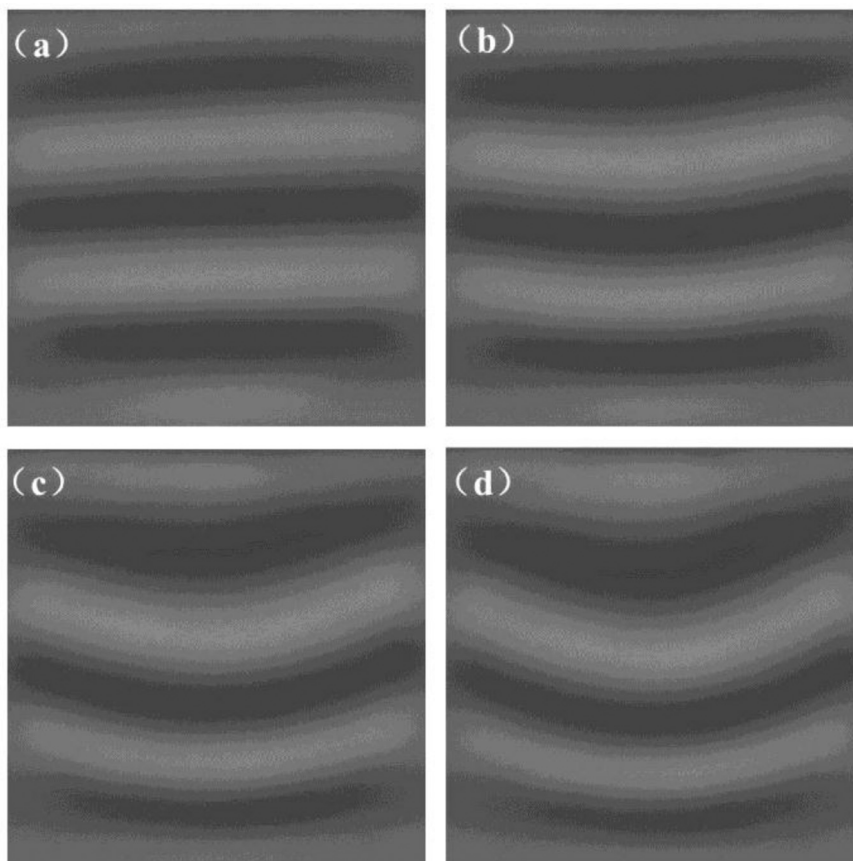


Fig. 8. The digital moiré obtained at pressure: (a) 0 kPa, (b) 40 kPa, (c) 80 kPa, (d) 100 kPa.

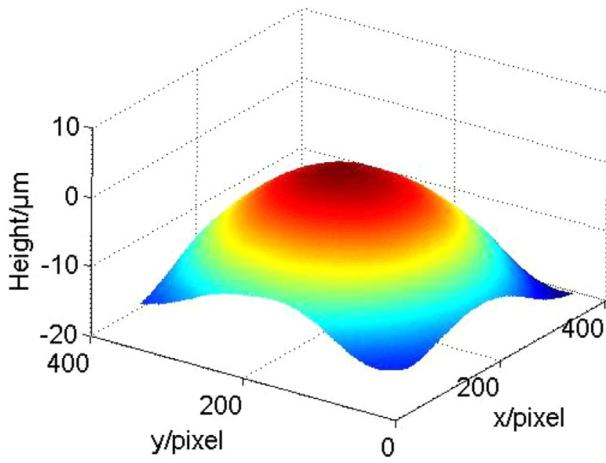


Fig. 9. The measured bulge deflection of the polyimide film at 25 °C and pressure 100 kPa.

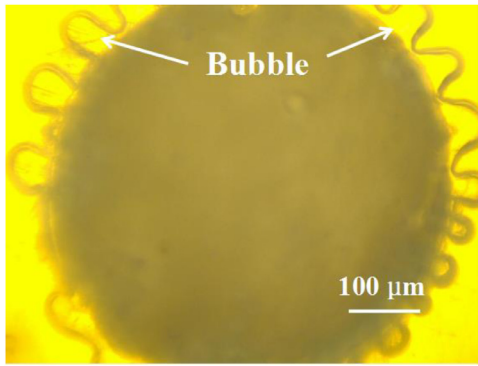


Fig. 10. The occurrence of the bubbles at pressure of 140 kPa.

of the bulge-deflection, the geometrical parameters and the mechanical properties (Young’s modulus and Poisson’s ratio) is established based on the hemispherical cap model of the bulged film [30]. It is assumed that the film was in a plane before the pressure is imposed. The radial stress σ_r in the isotropic film is:

$$\sigma_r = \frac{Pr^2}{4h_{\max}t} \quad (11)$$

where P is the pressure imposed to the film, and r is the radius of the bulged film, h_{\max} is the maximum deflection of the film and t is the thickness of the film. The radial strain was deduced as:

$$\epsilon_r = \frac{2h_{\max}^2}{3r^2} \quad (12)$$

From the tensile test conducted to the polyimide film, the stress-strain curve of the polyimide film approximates linear at initial segment. It has been evaluated from Eq. (11) the stress of the film at maximum pressure 100 kPa is in the approximate linear segment, so the linear elasticity model was applied to simplify the problem. The constitutive Equation can be expressed as:

$$\sigma_r = M\epsilon_r + \sigma_0 \quad (13)$$

where $M=E/(1-\mu)$, and is the biaxial modulus. E and μ are the elastic modulus and Poisson’s ratio. μ is known to be 0.34. (thought as known and is 0.34.) σ_0 is the initial radial residual stress in the film. It can be obtained from above equations:

$$P = M \frac{8t}{3r^4} h_{\max}^3 + \frac{4t\sigma_0}{r^2} h_{\max} \quad (14)$$

For the study of this paper, the residual stress σ_0 at the initial state is regarded as 0. So Eq. (8) was simplified as:

$$P = M \frac{8t}{3r^4} h_{\max}^3 \quad (15)$$

From Eq. (8), the maximum deflection can be obtained through calculating the phases of the gratings. With the pressure monitored from the control box, the elastic modulus can be measured.

The bulged deflection (Fig. 9) from 20 kPa to 100 kPa can be measured with Eq. (8), and the profile across the center-line of the bulged film measured with the proposed method is shown in Fig. 11. The maximum deflection h_{\max} of the bulged film can be extracted. From Fig. 11, the deflection is increasing with the growth of the pressure. With Eq. (15), the biaxial modulus can be calculated from the maximum deflection. Then the elastic modulus can be estimated.

The experimental result for the elastic modulus tested at 25 °C and 150 °C is shown in Fig. 12 respectively. It can be seen that the measured elastic modulus of the polyimide film at 150 °C is less than that at 25 °C. The average value of the elastic modulus is 0.94 GPa at 25 °C, and is 0.68 GPa at 150 °C, indicating that the elastic modulus of the polyimide film is lowered relatively at 150 °C.

The elastic modulus of the polyimide film from tensile test is about 0.9 GPa. It has been declared that the working temperature of the polyimide film can withstand more than 200 °C in the previous reports. Nevertheless, the mechanical property is reduced inevitably at 150 °C from the experimental result. The elastic modulus is reduced by 27% at 150 °C compared with that at 25 °C. In some cases, this level of decline of the mechanical properties may affect the performance of the polyimide films.

5. Conclusions

A micro-scale 3D deformation measurement method based on gratings and the optical microscope is proposed and applied to the bulge-test

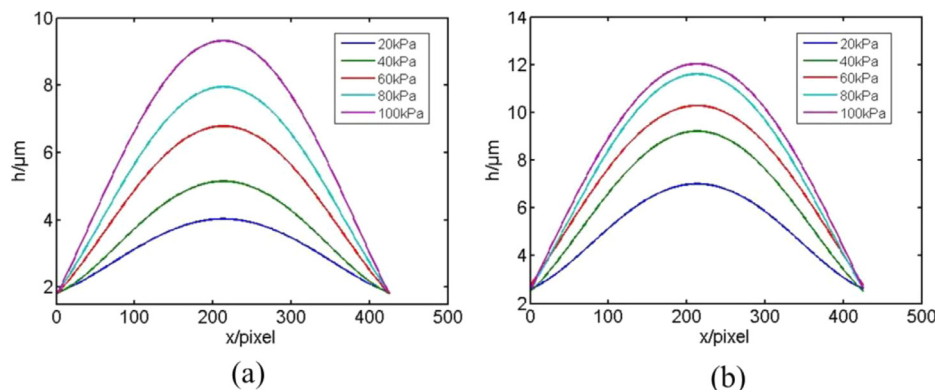


Fig. 11. The profiles across the center-line of the bulged film, (a) tested at 25 °C, (b) tested at 150 °C.

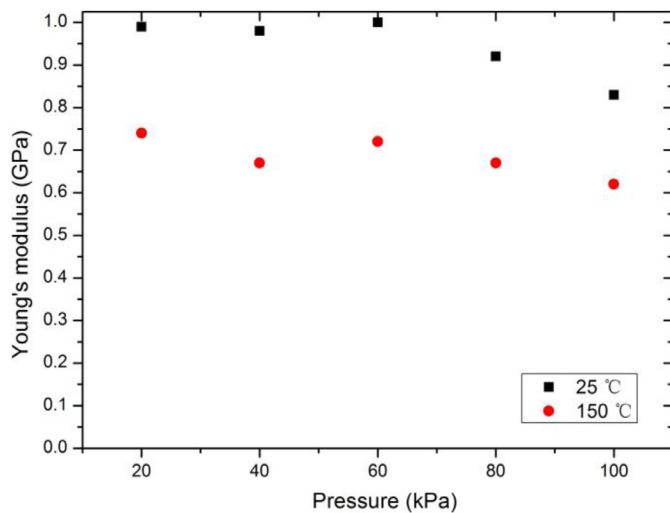


Fig. 12. The measured elastic modulus of the polyimide film at 25 °C and 150 °C.

to characterize the mechanical properties of the thin films. A micro-scale bulge-test apparatus was exploited. Thermal/mechanical coupling circumstance was incorporated in this bulge-test apparatus.

The error source and measurement accuracy of the proposed method is analyzed and estimated. The out-of-plane displacement accuracy is about 0.18 μm for the experiment conducted in this paper by the proposed method. It has been concluded that the accuracy of this method primarily depends on the grating frequency. It means the measurement accuracy increases with the increase of the grating frequency at the same deformation field.

With the proposed 3D deformation measurement method, the membrane bulge deflection was obtained. Combined with the bulge-test theory, the mechanical property of the film was evaluated. The polyimide films were tested at room temperature (25 °C) and 150 °C respectively. The experimental results indicate that the elastic modulus of the polyimide films was reduced 27% at 150 °C compared with that at room temperature.

The experimental results indicate that the proposed method is feasible for the bulge deflection measurement at micro-scale. It is also suggested that the method is promising in micro-scale 3D deformation measurement in other fields.

Acknowledgement

The authors are grateful to the financial support from the National Natural Science Foundation of China (Grant Nos. 11672153, 11232008, 11672141, 1172141).

References

[1] Pociavsek L, Dellsy R, Kern A, Johnson S, Lin B, Lee KYC, et al. Stress and fold localization in thin elastic membranes. *Science* 2008;320:912–16.

[2] Shang Y, Ye X, Feng J, Zhou H, Wang Y. Fabrication and characterization of a polymer/metal bimorph microcantilever for ultrasensitive thermal sensing. *IEEE Sens J* 2014;14:1304–12.

[3] Franklin AD. Nanomaterials in transistors: From high-performance to thin-film applications. *Science* 2015;349:704–+.

[4] Yin J, Zhao YP, Zhu RZ. Molecular dynamics simulation of barnacle cement. *Mater Sci Eng A* 2005;409:160–6.

[5] Nix WD. Mechanical properties of thin films. *Metall Trans A* 1989;20:2217–45.

[6] Shan ZH, Sitaraman SK. Elastic-plastic characterization of thin films using nanoindentation technique. *Thin Solid Films* 2003;437:176–81.

[7] Xiang Y, Chen X, Vlassak JJ. Plane-strain bulge test for thin films. *J Mater Res* 2005;20:2360–70.

[8] Sharpe WN Jr, Yuan B, Vaidyanathan R. New test structures and techniques for measurement of mechanical properties of MEMS materials. *SPIE Proc* 1996;2880:78–91.

[9] Li Y, Tang M, Xie H, Zhu R, Luo Q, Gu C. A measuring system for mechanical characterization of thin films based on a compact in situ micro-tensile tester and SEM moiré method. *J Micromech Microeng* 2013;2:085021.

[10] Cerda E, Mahadevan L. Geometry and physics of wrinkling. *Phys Rev Lett* 2003;90:074302.

[11] Kalkman AJ, Verbruggen AH, Janssen GCAM, Radelaar S. Transient creep in free-standing thin polycrystalline aluminum films. *J Appl Phys* 2002;92:4968–75.

[12] Lee H, Jung B, Kim D, Park H. On the size effect for micro-scale structures under the plane bulge test using the modified strain gradient theory. *Int J Pr Eng Man* 2011;12:865–70.

[13] Gruber PA, Böhm J, Onuseit F, Wanner A, Spolenak R, Arzt E. Size effects on yield strength and strain hardening for ultra-thin Cu films with and without passivation: a study by synchrotron and bulge test techniques. *Acta Mater* 2008;56:2318–35.

[14] Roussel M, Malhaire C, Deman A-L, Chateaux J-F, Petit L, Seveyrat L, et al. Electromechanical study of polyurethane films with carbon black nanoparticles for MEMS actuators. *J Micromech Microeng* 2014;24:055011.

[15] Berdova M, Ylitalo T, Kassamakov I, Heino J, Törmä PT, Kilpi L, et al. Mechanical assessment of suspended ALD thin films by bulge and shaft-loading techniques. *Acta Mater* 2014;66:370–7.

[16] Neggers J, Hoefnagels JPM, Hild F, Roux S, Geers MGD. Direct stress-strain measurements from bulged membranes using topography image correlation. *Exp Mech* 2014;54:717–27.

[17] Yu Z, Mao W, Li F, Feng X, Pei Y, Fang D. Magnetic and electric bulge-test instrument for the determination of coupling mechanical properties of functional free-standing films and flexible electronics. *Rev Sci Instrum* 2014;85:065117.

[18] Li C, Liu Z, Xie H. Novel scanning electron microscope bulge test technique integrated with loading function. *Rev Sci Instrum* 2014;85:103709.

[19] Cao Z, Wang P, Gao W, Tao L, Suk JW, Ruoff RS, et al. A blister test for interfacial adhesion of large-scale transferred graphene. *Carbon* 2014;69:390–400.

[20] Jia HK, Wang SB, Li LA, Wang ZY, Goudeau P. Application of optical 3D measurement on thin film buckling to estimate interfacial toughness. *Opt Lasers Eng* 2014;54:263–8.

[21] Larsson L, Sjödal M, Thuvander F. Microscopic 3-D displacement field measurements using digital speckle photography. *Opt Lasers Eng* 2004;41:767–77.

[22] Shi HJ, Ji HW, Yang GB, He XY. Shape and deformation measurement system by combining fringe projection and digital image correlation. *Opt Lasers Eng* 2013;51:47–53.

[23] Wu D, Xie H, Li C, Wang R. Application of the digital phase-shifting method in 3D deformation measurement at micro-scale by SEM. *Mea Sci Tech* 2014;25:125002.

[24] Tang M, Xie H, Zhu J, Li X, Li Y. Study of moiré grating fabrication on metal samples using nanoimprint lithography. *Opt Express* 2012;20:2942–55.

[25] Li Y, Xie H, Guo B, Luo Q, Gu C, Xu M. Fabrication of high-frequency moiré gratings for microscopic deformation measurement using focused ion beam milling. *J Micromech Microeng* 2010;20:055037.

[26] Yokozeki S, Kusaka Y, Patorski K. Geometric parameters of moiré fringes. *Appl Opt* 1976;15(9):2223–7.

[27] Creath K, Schmit J. N-point spatial phase-measurement techniques for non-destructive testing. *Opt Lasers Eng* 1996;24(5-6):365–79.

[28] Xu D, Liecht KM. Bulge testing transparent thin films with moiré deflectometry. *Exp Mech* 2010;50:217–25.

[29] Xing YM, Kishimoto S, Shinya N. Multiscanning method for fabricating electron moiré grating. *Exp Mech* 2004;44:562–6.

[30] Beams JW. Structure and properties of thin films: proceedings of an international conference. New York: Neugebauer C A; 1959.